Cryst. Res. Technol. 49, No. 1, 43–54 (2014) / DOI 10.1002/crat.201300430

CRYSTAL Research & Technology

Review Article

Probing a crystal's short-range structure and local orbitals by Resonant X-ray Diffraction methods

Matthias Zschornak[1,*], *Carsten Richter*[1], *Melanie Nentwich*[1], *Hartmut Stöcker*[1], *Sibylle Gemming*[2], *and Dirk C. Meyer*[1]

Received 20 December 2013, revised 31 December 2013, accepted 2 January 2014
Published online 27 January 2014

Diffraction Anomalous Fine Structure (DAFS) combines the long-range, crystallographic sensitivity of X-ray diffraction with the short-range sensitivity of *X-ray Absorption Spectroscopy* (XAS). In comparison to other spectroscopic methods, DAFS can additionally distinguish phases of different translational symmetry by choice of momentum transfer, or isolate spectra from chemically identical atoms on various Wyckoff sites of a crystal's structure using crystallographic weights. The *Anisotropy of Anomalous Scattering* (AAS) extends the concept of isotropically scattering atoms to a more general case, where the atom's scattering characteristics depend on the polarization as well as the wavevector of the incident and scattered X-rays. These can be written as tensors that reflect the local site symmetries of the resonant atom. *Forbidden Reflection Near-Edge Diffraction* (FRED) is an elegant way to measure AAS by using reflections that are extinguished in the special case of isotropically scattering atoms. They can only be observed due to the non-isotropic contributions at photon energies in the vicinity of an absorption edge where electronic transitions occur. Combining the site selectivity of DAFS with the information accessible through AAS allows probing the short-range order and local orbitals of selected atoms in a crystal structure of a chosen phase. The present condensed review gives a brief overview on the pioneer work, the theory and sensitivities as well as selected recent applications of these powerful and promising *Resonant X-ray Diffraction* (RXD) methods. Additionally, some recent work of the authors is included exemplarily for the model structure rutile TiO_2 presenting the progress in measurement and interpretation.

1 Introduction

X-ray diffraction is a well-established tool for the determination of crystalline structures and electron density distributions at the atomic scale. It has been extended by the use of "anomalous" or "resonant" scattering techniques, to enable a detailed study of the electronic and magnetic properties of certain atoms in the structure (*e.g.* [1]), to solve the phase problem [2–4] or to gain more information by changing the scattering contrast between the different scatterers [5, 6]. In order to make use of these techniques, the energy of the incident photons has to be tuned close to that of an electronic transition in the atom of interest. As a consequence, the interaction of X-rays with the resonant atom becomes much more sensitive on the polarization of the incident and scattered photons, so that it may not be regarded as isotropic anymore. The development of modern synchrotron light sources made resonant diffraction a more widely used method, since they offer a wide, continuous range of X-ray wavelengths and a well-defined polarization state of the incident photons. In the present condensed review these phenomena are highlighted with the focus on the study of electronic properties of certain atoms, such as unoccupied valence orbitals, which are determined by its local structure, like nearest neighbor distances, local symmetries, etc.

* Corresponding author: e-mail: matthias.zschornak@physik.tu-freiberg.de; Tel: +49 (0) 3731 39 2865, Fax: +49 (0) 3731 39 4314.
[1] TU Bergakademie Freiberg, Institut für Experimentelle Physik, Leipziger Str. 23, 09596 Freiberg, Germany
[2] Helmholtz-Zentrum Dresden-Rossendorf, Institut für Ionenstrahlphysik und Materialforschung, Bautzner Landstraße 400, 01328 Dresden, Germany

CRYSTAL Research & Technology

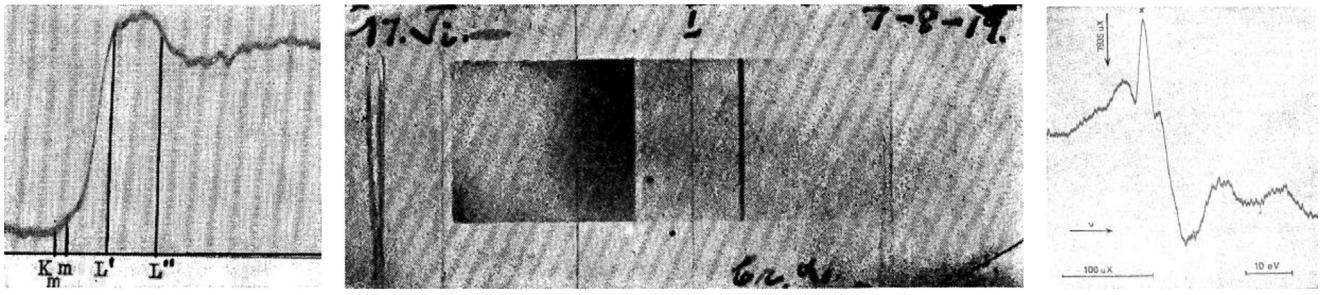

Fig. 1 Discovery of the "Fine Structure of Absorption" (*i.e.* XAFS) in 1920 by Fricke at the *K*-edges of several elements – here shown for the titanium edge of TiO_2 (left and middle) and discovery of "raie de diffusion anomales" (*i.e.* DAFS) in 1956 by Cauchois for the 002 reflection at the *K*-edge of aluminum (right). For full details, we refer the reader to the original publications [7, 13]. Reprinted with permission from H. Fricke, Phys. Rev. **16**, 202 (1920) and Y. Cauchois, C. R. Acad. Sci. (Paris) **242**, 100 (1956). Copyright (1920) by the American Physical Society and (1956) by the Académie des sciences.

2 History and present status

2.1 Pioneer work

X-ray Absorption Fine Structure (XAFS) has been first noticed by Fricke in 1920 [7] (see figure 1, left and middle). Since the development of second generation synchrotron sources, it has become a powerful method for short-range structure refinement (see *e.g.* [8–11]). Bijvoet used *Anomalous Scattering* and the breaking of Friedel's Law in the resonance case for phase determination in 1949 [3], which today is used for the technique of *Multi-Wavelength Anomalous Diffraction* (MAD) [12] – a method to solve the phase problem of crystallography for standard structure determination based on Bragg reflection intensities. Energy dependencies of the diffracted intensities of crystals similar to XAFS have been first found by Cauchois in 1956 [13] (see figure 1, right), which have been later called *Diffraction Anomalous Fine Structure* (DAFS). More than 30 years later, in the 1980's and 90's there had been significant research to extend the absorption based concept to diffraction, *i.e.* to make use of the momentum transfer in order to select certain phases of the probed volume or certain Wyckoff positions within a crystal structure [14–27]. In the vicinity of absorption edges, an enhanced sensitivity of the X-rays is observed which can be used to study the coupling of electronic and magnetic properties with structure (*e.g.* Dzyaloshinskii-Moriya interaction [28], see section 2.2). A more exhaustive review on early DAFS work was written by Sorensen *et al.* [19] and also by Renevier *et al.* covering the technical achievements [29]. DAFS exploits the energy dependent intensity of certain Bragg reflections of crystals and, thus, it does not average over all resonantly scattering atoms in the unit cell, but it exclusively collects information of the corresponding subset of resonant scatterers selected by the Bragg condition (see section 4).

Templeton & Templeton studied the polarization dependence of *Resonant X-ray Scattering* experimentally, in 1980 on Vanadyl Bisacetylacetonate in absorption [30] and in 1982 on a rubidium uranyl nitrate in diffraction [31], which later got known as *Anisotropy in Anomalous Scattering* (AAS). They suggested that AAS can cause the excitation of reflections forbidden by symmetry based on translational components in the space group (*i.e.* screw axes or glide planes) for spherical atomic scattering factors, as stated *e.g.* in the *International Tables for Crystallography A* [32]. The theoretical basis for these "forbidden" reflections, also termed *Forbidden Reflection Near-Edge Diffraction* (FRED) [33], was developed by Dmitrienko in 1983 [34] and they were first observed by Templeton & Templeton for cubic $NaBrO_3$ in 1985 [35] and later found on several other crystals, *e.g.* by Eichhorn *et al.* for Cu_2O [36] and Kirfel & Petcov for TiO_2 [37], see topical review [38].

With the change of the century an increasing number of researchers from the field of neutron scattering were attracted by the growing availability of these *Resonant X-ray Diffraction* synchrotron methods, which accounts for the recent focus on studies of magnetism using *X-ray Magnetic Circular Dichroism* (XMCD), and both communities are experiencing a process of joining since. For a detailed summary of related work from both fields see for instance the review of Beale *et al.* [39].

2.2 Recent advances

In the following, a selection of recent work from the last three years related to DAFS and Resonant Scattering methods is reviewed.

CRYSTAL Research & Technology

In 2010, Staub *et al.* [40] performed AAS and DAFS scans at the Fe *K*-edge of $GaFeO_3$. Probing forbidden reflections, they were able to test magnetoelectric multipole moments directly. A sign change in the magnetic signal of the Friedel-pair $0k0$, $k = \pm 5$ and the azimuthal dependence could be attributed to the interference of an electric quadrupole with magnetoelectric quadrupole and octupole moments. The comparable *Soft X-ray Resonant Diffraction* (SXRD) and *Neutron Powder Diffraction* (NPD) analysis of the manganates $Nd_{0.4}Tb_{0.6}BaMn_2O_6$ and $SmBaMn_2O_6$ exhibited a similar dependence on doping the *A*-site of the perovskite with divalent cations and increasing the temperature [41].

Azimonte *et al.* [42] were able to detect minor polar atomic displacements in multiferroics using anomalous X-ray diffraction at the Mn *K*-edge of $DyMn_2O_5$ while additionally applying an electric field with switchable polarization. Comparison of DAFS and XAFS scans of the Friedel-pair 362/-3-6-2 (due to the different polarization) displays a large effect directly correlated with a displacement of the Mn ions. Beale *et al.* [43] performed a direct measurement of the antiferromagnetic spin polarization at the O sites of $TbMn_2O_5$ by analyzing the $\frac{1}{2}0\frac{1}{4}$ reflection (fractional indices here and later on with respect to the main lattice) at the Mn L_3- and O *K*-edge with AAS scans. They were also able to show the correlation of increased ordering of spin polarization and the displacement of the Mn ion from the base into the coordination pyramid. Souza *et al.* [44] used *Resonant Soft X-ray Diffraction* for studying the Mn and O sublattices and their interaction within RMn_2O_5 (R = Y, Er). The azimuthal scan (AAS) at the $\frac{1}{2}0\frac{1}{4}$ forbidden reflection at the Mn L_3-edge can be described with a tensor of rank 1, and is thus a magnetic dipole.

In general, *Resonant X-ray Scattering* is an important tool for the investigation of antiferromagnetic or even multiferroic materials. Walker *et al.* [45] have exploited the magneto-electric coupling in multiferroic $TbMnO_3$, and hence, the interference between charge and magnetic X-ray scattering to resolve the ionic displacements and their contribution to the zero-field ferroelectric moment. This field includes theoretical predictions of new physical phenomena (*e.g.* [46]) and extends towards inelastic X-ray scattering (*e.g.* [47]). The research of Haverkort *et al.* [48] revealed the importance of using a rather precise symmetry instead of a spherical one for simulations, by comparing calculations based on different models. One of the examples was the artificial superlattice of six NiO layers alternating with one MnO layer. For the first Bragg reflection, the calculations for a cubic and aspherical symmetry were compared, revealing significant differences.

Pascut *et al.* [49] used DAFS at the Ni *K*-edge of single crystalline $2H$-$AgNiO_2$ to test the model of charge ordering (CO) as alternative approach to the Jahn-Teller effect. The "honeycomb" CO can be interpreted as $a_0\sqrt{3} \times a_0\sqrt{3} \times c$ superstructure and causes a splitting of the Ni positions in an electron-rich one Ni_1 and two electron-depleted positions $Ni_{2,3}$. Using a fit of the DAFS data to extract $f'(E)$ and i$f''(E)$ for Ni_1 and $Ni_{2,3}$ depicts a shift of the Ni edge of about 2.5 eV, implicating a core hole shift of 1 eV. This shift confirms the predicted difference in electron density. Band structure calculations involving CO and hybridization of Ni and O could explain the change in the electronic energy levels of Ni.

In 2011, Herrero-Martìn *et al.* [50] investigated the phase transition of $La_{0.5}Sr_{1.5}MnO_4$ from tetragonal $I4/mmm$ to an orthorhombic phase while lowering temperature, accompanied by a semiconductor-insulator transition. Using DAFS scans at $h/2h/2l$ and $h/4h/4l$ superstructure reflections of the tetragonal phase (h odd and l even) as well as their azimuthal dependence they were able to confirm the transition to space group *Cmcm* involving three active modes, which cause a shift of the oxygen atoms.

Beside the regular combination of DAFS with the method XAFS there were some efforts to join the advantages of DAFS with those of other methods. Tuilier *et al.* [51] determined the environment of Ti atoms in $Ti_{1-x}Al_xN$ for $x = 0.0$, 0.5 and 0.68. Using *X-ray Absorption Near Edge Spectroscopy* (XANES), they were able to determine a hexagonal lattice for $x = 0.68$. A shoulder in the pre-edge region gave hint to a superposition of hexagonal and cubic environments, which could be confirmed by *Diffraction Anomalous Near-Edge Spectroscopy* (DANES). With this experiment the pre-edge shape of Ti in tetrahedral coordination in nitrides could be determined. Favre-Nicolin *et al.* [52] gave a review on the combined usage of *Multi-Wavelength Anomalous Diffraction* (MAD) and DAFS, *e.g.* for determining the diffusion of Si into Ge quantum dots on Si bulk and the growth mechanisms of AlGaN/Si(111) nanowires. In the last years, DAFS has mainly been used on micro-structures like thin films [51, 52], nano-islands [52] and quantum dots [52, 53].

In 2011, Walker *et al.* used AAS for investigations of the "hidden order" arising during the specific-heat anomaly of URu_2Si_2. By comparing simulated and experimental AAS curves of the 201 reflection at the uranium M_4-edge they were able to exclude quadrupolar effects within a certain range of propagation vectors [54]. Walker *et al.* were also scanning the uranium M_4-edge of $U(Pd_{1-x}Pt_x)_3$ ($x = 0.005$, 0.01) [55]. For $x = 0$ there are four different phase transitions below 8 K, the

CRYSTAL Research & Technology

lowest two influenced by an ordering of the uranium 5*f* electrons, accompanying an in-phase stacking Q_{xy} and causing super-lattice reflections. The AAS scan of the 104 superlattice reflection for $x = 0.005$ and simulations for Q_{xy} showed good agreement, but no 104 reflection could be detected for $x = 0.01$. This implicates that 0.5% Pt-doping leaves 5*f* electron ordering unchanged whereas 1% doping prevents the ordering and thus the superstructure reflections.

Recently, AAS was used for the analysis of the metal-insulator transition of $Sr_3(Ru_{1-x}Mn_x)_2O_7$ [56, 57]. The azimuthal scans of the $^1/_4{}^1/_4 0$ structurally forbidden reflection were applied at the *L*-edges of Mn and Ru. Remarkably, the Mn edge is more sensitive for the magnetic superstructure than the Ru edge. Hossain *et al.* were able to show the existence of a global spin correlation of the randomly distributed Mn atoms within the crystal, despite of their diluted concentration [57]. Concluding from the independence of the superstructure reflection of the Mn concentration, the ordering is mainly of electronic nature and the Mn atoms do essentially trigger this effect [56].

A review about recent developments applying AAS and forbidden reflections can be found in Kokobun *et al.* [58]. In 2012, further reviews appeared on the occasion of the *Resonant Elastic X-ray Scattering* workshop 2011 concerning the development within the last 20 years in general [39, 59] and with specific focus on actinide systems [60], theoretical aspects [61] as well as polarization analysis [62].

2.3 Development and improvement of calculations and models

The modeling of atomic scattering factors *f* and related matrix elements for electronic transitions from core states into vacant intermediate states started from the application of the optical theorem [63, 64]. Cromer and Libermann improved the oscillator-strength based calculations of the corrections f' and if'' (see section 3) by using self-consistent field relativistic Dirac-Slater wave functions [65, 66]. After the introduction of Fourier analysis for the description of EXAFS [8], McKale *et al.* published exhaustive data on backscattering amplitude and phase functions derived from *ab initio* calculations for the whole periodic table [67]. Kolpakov *et al.* and later Dmitrienko extended the dielectric tensor formalism to the X-ray energy regime [34, 68] to account for the polarization dependence of resonant X-ray scattering. A concept for the calculation of dynamic electron excitations into several intermediate states within the frame of the *Multiple Scattering Theory* is discussed by Natoli *et al.* [69] and implemented into the code FEFF by Rehr *et al.* [70]. The code has also been made applicable to diffraction in later versions [71], although similarities in the analysis of absorption and diffraction had been suggested much earlier [72]. The implemented formalism based on Green's functions was improved by Ankudinov and Rehr, which eliminated the necessity of using the so far applied Kramers-Kronig relation [73,74]. Benfatto and Felici applied an equivalent approach for the calculation of tensorial atomic scattering factors [75]. With the introduction of the FDMNES code by Joly *et al.* [76, 77], which is based on the *Finite Difference Method* (FDM) and solves Schrödinger's equation for a cluster of atomic potentials, a formalism beyond the muffin-tin approximation with highly improved accuracy for the *X-ray Absorption Near Edge Structure* (XANES) spectral region was derived. Further enhancement could be made by the implementation of self-consistency of electronic states and effective potential (see *e.g.* [78]). Alternative approaches abandon the explicit treatment of excited states, *e.g.* by the implementation of a polarization propagator into *Density Functional Theory* (DFT) [79], or go beyond the independent particle approximation, *e.g.* within the time-dependent DFT picture or by treating the core-hole according to the Bethe-Salpeter theory (for a review see *e.g.* [80]).

2.4 Measurement setup

Resonant X-ray scattering experiments are performed at synchrotrons, on the one hand for their need of high photon flux and on the other hand, even more important, for the requirement of continuously tunable photon energy. Besides X-ray source (bending magnet, wiggler or undulator) and diffractometer (in Euler or Kappa geometry with a minimum of 4 circles), instrumentation in general includes a double-crystal monochromator to scan the energy, a primary beam intensity monitor to normalize the intensities, a point detector (scintillator or avalanche diode) for recording the reflection intensities and an energy-dispersive detector for a simultaneous measurement of X-ray fluorescence to obtain the absorption (see figure 2). For a full polarization analysis, an analyzer crystal can be installed in front of the detector and the sample can be rotated around the $\boldsymbol{q}$-vector (see figure 2, right), *e.g.* by using a 6-circle diffractometer [81], or the incident radiation polarization may be changed using a phase retarder and phase plates [82], or by turning the whole diffractometer [83].

CRYSTAL Research & Technology

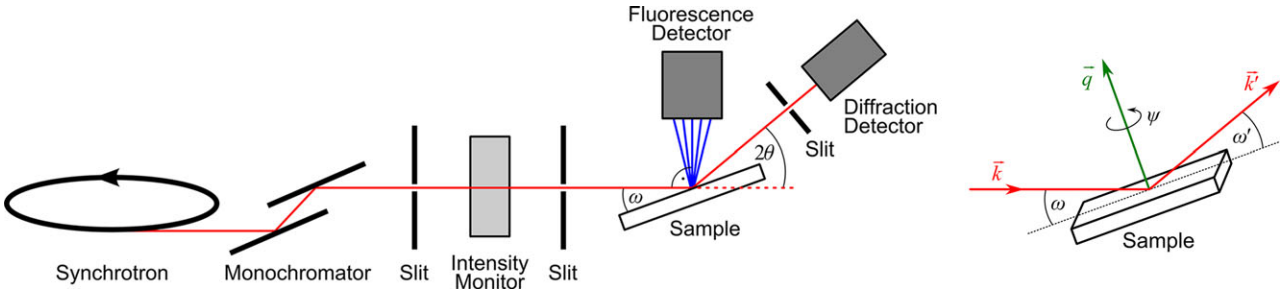

Fig. 2 General experimental setup of a Resonant X-ray scattering measurement (left) recording the diffraction as well as the absorption signal. For polarization analysis the azimuthal dependence ψ reflects the crystal's orientation for a fixed momentum transfer $\boldsymbol{q} = \boldsymbol{k}'\text{-}\boldsymbol{k}$ with respect to the polarization states of the incident X-rays with wavevector $\boldsymbol{k}$ (right).

3 Theory of Resonant X-ray Diffraction

3.1 Resonant Elastic X-ray Scattering

Resonance in X-ray scattering means that at absorption edges of a certain atomic species the energy of the incident X-rays meets the atom's energy differences or eigenenergies. For that specific species in the crystal structure the atomic scattering factor f obtains complex energy dependent contributions $f'(E)$ and $\mathrm{i}f''(E)$ as corrections $\Delta f(E)$ to the Thomson scattering $f_0(q)$, which resembles the Fourier transformed atomic electron density. The corrections result from transitions of electrons from core states $|\phi_i$ of energy E_i to unoccupied intermediate states $|\phi_f$ of energy E_f and lifetime $\hbar/\Gamma_f$ becoming strong for a high density of those states. These intermediate valence states are influenced by electronic interactions within the local atomic environment *i.e.* short-range order of the resonant scatterer, which can cause a deformation of the valence states similar to bonds of occupied states. Thus, absorption and diffraction become anisotropic, depending on the crystal's orientation with respect to incident and scattered X-ray polarization vectors $\boldsymbol{\varepsilon}$ and $\boldsymbol{\varepsilon}'$ (with wavevectors $\boldsymbol{k}$ and $\boldsymbol{k}'$, momentum operator $\boldsymbol{p}$, photon energy $\hbar\omega$, electron mass m_e) as given by:

$$\Delta f(\omega, \boldsymbol{k}, \boldsymbol{k}') = \frac{1}{m_e} \sum_f \frac{\langle\phi_i|(\boldsymbol{\varepsilon}'\cdot\boldsymbol{p})\mathrm{e}^{-\mathrm{i}\boldsymbol{k}'\boldsymbol{r}}|\phi_f\rangle\langle\phi_f|(\boldsymbol{\varepsilon}\cdot\boldsymbol{p})\mathrm{e}^{\mathrm{i}\boldsymbol{k}\boldsymbol{r}}|\phi_i\rangle}{\hbar\omega - (E_f - E_i) + \mathrm{i}\Gamma_f/2}. \tag{1}$$

The atomic scattering factor can be expanded into a series of tensors – dipole-dipole, dipole-quadrupole, quadrupole-quadrupole *etc.* – which leads to a tensorial structure factor as well (see *e.g.* [61]).

The polarization dependence and the exhibited anisotropy can be of different nature. Contributions can be caused by:

1. non-spherical electron density distributions of one species of atoms [84],
2. excitation of electron core states to statically deformed intermediate states due to anisotropic charge transfer to the local atomic neighborhood (*e.g.* in cubic $NaBrO_3$ [35] or TiO_2 [37]),
3. static displacement of resonant scatterers and the resulting deformation of intermediate electronic states due to point defects [85, 86] or the Jahn-Teller effect [87],
4. dynamic displacements caused by thermal motion, which takes into account the temperature dependent displacement of the resonant scatterer's core state [88], and phonons [50].

Thermal vibration as well as point defects like vacancies or substitutional and interstitial atoms deform the regular crystal structure, in the position and symmetry of the defect and defect-near atoms and, more severely, in the local electronic states. As seen from equation (1) these changes in the unoccupied states result in altered or new resonant scattering transitions, which are known as *thermal-motion-induced* (TMI) and *point-defect-induced* (PDI) contributions to the intensity (see *e.g.* [85, 89]).

3.2 Forbidden reflections

A direct consequence of the polarization dependence is that certain reflections, forbidden in a space group due to symmetry elements with a translational part (screw axes or glide planes), become symmetry allowed when taking into account polarization (and wavevector) dependence of the scattering amplitude f as described by equation (1). This way, these purely resonant reflections reveal peculiarities beyond charge density, such as orbital ordering [90], magnetic ordering and the chirality of crystals, as discussed theoretically [91] and observed *e.g.* on

CRYSTAL Research & Technology

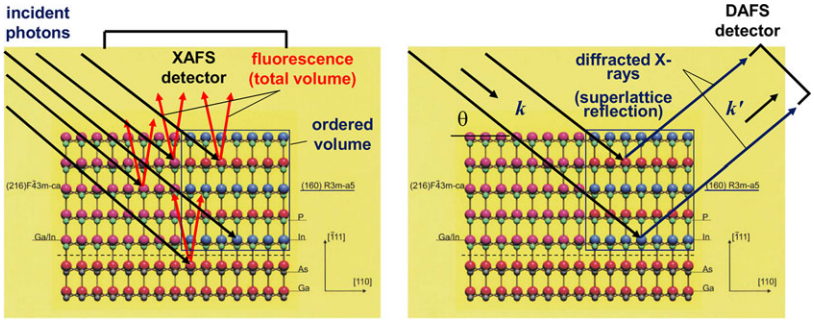

Fig. 3 Difference of XAFS signal (left) and DAFS signal (right). Whereas the fluorescence from the Ga absorption is collected integrally over all ordered and randomly distributed Ga atoms, the diffracted intensity originates exclusively from the ordered phase of the sample chosen by the according momentum transfer of the super lattice – also known as wavevector selectivity. For full details, we refer the reader to the original publication [23]. Reprinted with permission from D. C. Meyer *et al.*, J. Synchrotron Rad. **5**, 1275 (1998). Copyright (1998) by the International Union of Crystallography.

right- and left-handed alpha-quartz enantiomers [92]. Since the spherical parts of the non-resonant as well as the resonant scattering contributions cancel out by destructive interference, "forbidden" reflections only depend on the anisotropic part of the atomic scattering tensor *f*. Therefore, these reflections represent a unique experimental access to study the local environment of resonant scatterers and their electronic states. Not all structures exhibit these translational symmetry elements but polarization analysis is not restricted to "forbidden" reflections and in principle occurs on allowed reflections as well, although with restricted signal-to-noise ratio.

4 Applications of Diffraction Anomalous Fine Structure

4.1 Wavevector Selectivity

DAFS can be used to distinguish atoms of the same species within different structural phases by means of the wavevector. A certain phase is selected by matching its long-range periodicity with the momentum transfer $\boldsymbol{q} = \boldsymbol{k}'-\boldsymbol{k}$, *i.e.* by choosing the corresponding Bragg reflection, and elastic scattering contributions from other phases will not meet the particular Bragg condition and do not contribute to the signal.

Meyer *et al.* were performing DAFS measurements for structure and polarization analysis of a (Ga,In)P heterostructure which was epitaxially grown on (001)-oriented GaAs. GaInP exhibits a CuPt-structure with alternating Ga and In {111} planes (see figure 3). Selecting the GaInP Bragg reflections, they could isolate the fine-structure function of the Ga atoms present in that phase from those contained in the substrate, which helped to understand the ordering of Ga and In atoms within the {111} planes. This way, they could show that DAFS only contains the information about the short-range order of certain ordered phases of the structure chosen by the vector of momentum transfer [23] – a feature of DAFS that is known as wavevector selectivity. Furthermore, they recorded a significant influence of absence or presence of inversion symmetry on the DAFS signal, enabling structure analysis with this method.

4.2 Site Selectivity

Even more specific, the structure factor of a crystal structure is the coherent sum of the subsets of symmetrically equivalent atoms with a certain multiplicity, called Wyckoff positions. Each of these subsets has a contribution based on the positions of the associated atoms in the unit cell, which add up to the so called crystallographic weight of a subset. In general, the crystallographic weights vary when changing between Bragg reflections and can reach zero for a certain subset, if the reflection conditions of the specific Wyckoff position, as stated *e.g.* in the *International Tables for Crystallography Vol. A* [32], are not met. Thus, by measuring DAFS for a set of reflections, the spectra of the atomic scattering amplitude can be isolated and, consequently, local structure information can be obtained separately for each Wyckoff position.

This site-selectivity in resonant diffraction was shown, for example, by Nazarenko *et al.* [93], who studied magnetite Fe_3O_4 at the phase transition to its low temperature phase (*Pmca*). The structure consists

CRYSTAL Research & Technology

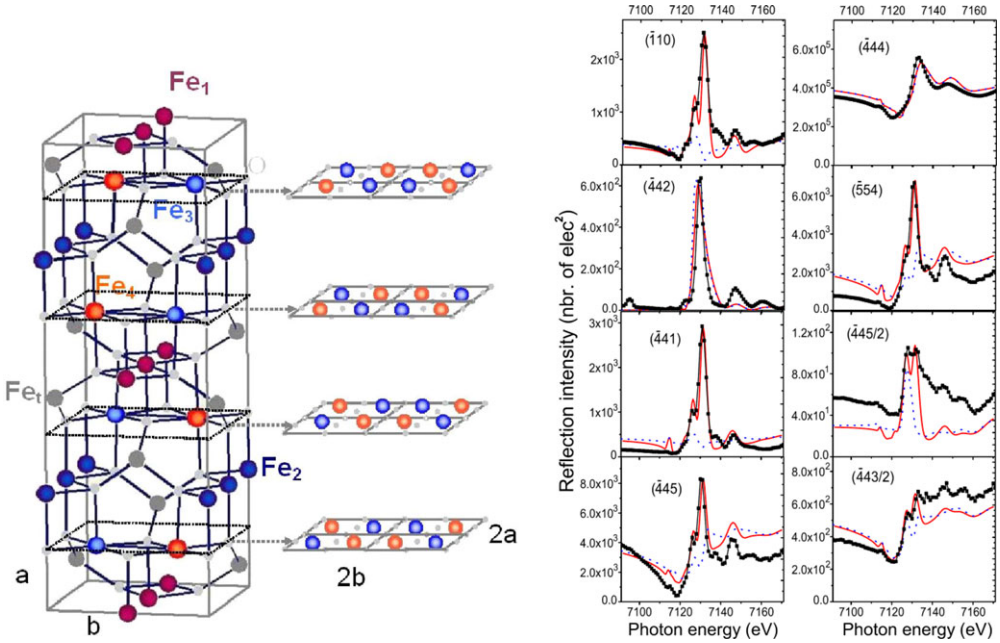

Fig. 4 Charge ordering (CO) in the low temperature phase of Magnetite Fe_3O_4 (*Pmca*) with six distinct iron Wyckoff positions (left): four octahedrally coordinated (Fe_{1-4}) showing CO and two tetrahedrally (Fe_t) without CO. The sensitivity of chosen Bragg reflections to the different iron sites can be seen in the resonantly diffracted intensities (right) for photon energies in the vicinity of the iron *K*-edge (black: experimental, red: calculated with CO, blue: calculated without CO). Some reflections as -110 and -441 are and some as 442 are not sensitive to CO, half-integer reflections as -445/2 depend on the charge difference between Fe_3 and Fe_4. For full details, we refer the reader to the original publication [93]. Reprinted with permission from E. Nazarenko *et al.*, Phys. Rev. Lett. **97**, 056403 (2006). Copyright (2006) by the American Physical Society.

of six symmetrically inequivalent iron sites, two in tetrahedral and four in octahedral coordination. At the Verwey phase transition, a charge disproportionation occurs between the iron atoms in octahedral coordination (see figure 4). The effect could be proven by resonant diffraction at the iron edge investigating several Bragg reflections with different crystallographic weights for each of these Wyckoff positions. By evaluation of the structure factor, reflections -110 and -441 turned out to be very sensitive while the reflection 442 is not sensitive at all to the charge ordering, whereas half-integer reflections as -445/2 depend, in

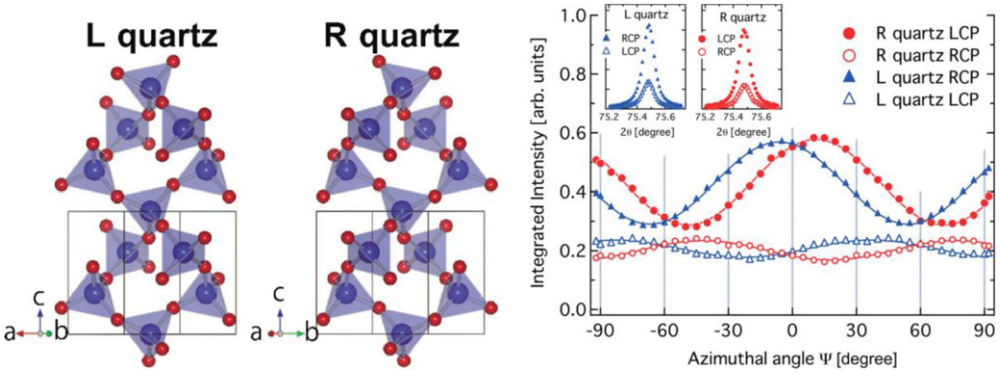

Fig. 5 Chirally opposite left and right handed quartz (left) rotates circularly polarized and diffracted X-rays differently. Tanaka *et al.* gave experimental proof (right) how resonant Bragg diffraction distinguishes enantiomers. For full details, we refer the reader to the original publication [92]. Reprinted with permission from Y. Tanaka *et al.*, Phys. Rev. Lett. **100**, 145502 (2008). Copyright (2008) by the American Physical Society.

CRYSTAL Research & Technology

particular, on the charge difference between iron sites Fe_3 and Fe_4.

Subsequent *Resonant X-ray Diffraction* experiments revealed further details of the interplay among electronic degrees of freedom (charge and orbital order), spin and lattice distortion that concur at the Verwey phase transition in magnetite. The lattice distortions developing in the low temperature phase were found to share the same symmetry as the orbital fluctuations, and therefore the Verwey transition may be described also as a kind of Jahn-Teller transition [94].

5 Applications of Anisotropic Anomalous Scattering

5.1 Determination of Chirality

Two structures are chiral to each other if they are mirroring each other and cannot be translated into each other by pure rotational operations (see figure 5, left). Tanaka *et al.* [95] developed a new method for determining the chirality of enantiomers of left and right handed quartz (space groups $P3_121$ (152) and $P3_221$ (154), respectively). Standard X-ray diffraction methods do not distinguish between chiral space groups. But using circular polarized X-ray beams in an AAS measurement they were able to differentiate the handedness of quartz berlinite and tellurium crystals. A more detailed description of the method has been already given before [92]. Both quartz types were probed with left- as well as right-circularly polarized (LCP and RCP) X-ray beams (see figure 5, right). The AAS of the 001 reflection for R quartz, LCP and L quartz, RCP are comparable in shape and amplitude, exhibiting a periodicity of 120° in ψ due to the threefold symmetry. The phase shifts for LCP and RCP show opposite sign with respect to $\psi = 0°$. Additional AAS measurements for L quartz at the 00-1 reflection revealed an antiphase relation between the integrated intensities of the 001 and the 00-1 reflection. By calculation of the intensities for all symmetries, a correlation between helicity and chirality was found.

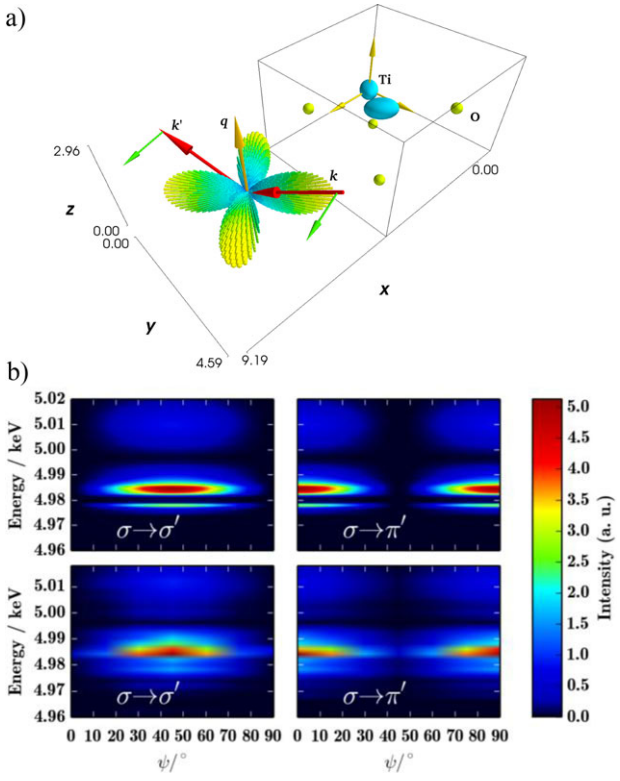

Fig. 6 a) Phenomenological simulation of the rutile 001 structure factor tensor in dependence on the polarization states. The tensor (left) is the coherent sum of the two aspherical Ti scattering ellipsoids (turquois) and four spherical O contributions (yellow) with geometric factors according to their positions in the rutile unit cell. Contraction with the polarization vectors (green) of incident and diffracted X-rays (red vectors), shown here for $\sigma - \sigma'$ geometry, yields the reflection intensity. b) The FDM calculation (upper panels) of electronic transitions in rutile according to equation (1) and convoluted intensity is based on a self-consistently refined charge transfer and potential and allows for an interpretation of scattering contributions with respect to the local orbital momentum resolved density of unoccupied electronic states (local PDOS). All features of the experimental DAFS-AAS data (lower panels) can be well described for the $\sigma - \sigma'$ as well as the $\sigma - \pi'$ channel.

5.2 Site Symmetry and Phase of the Resonant Scatterer and "Forbidden" Reflections

Rutile is the most stable allotropic modification of TiO_2 at room temperature and crystallizes in the space group $P4_2/mnm$ (136) with lattice parameters $a = 4.5925$ Å and $c = 2.9578$ Å. Within the tetragonal structure the titanium atom occupies an inversion center at the origin on the Wyckoff site 2*a* with local symmetry *m.mm*. This results in three complex tensorial degrees of freedom for the dipole-dipole part, $f^d{}_{11}$, $f^d{}_{33}$ and $f^d{}_{12}$, and further degrees of freedom for the quadrupole-quadrupole part of the atomic scattering factor, whereas dipole-quadrupole scattering remains forbidden. Dipole and quadrupole transitions from the 1s initial state probe unoccupied orbitals of p- and d-symmetry, respectively. Ti is

CRYSTAL Research & Technology

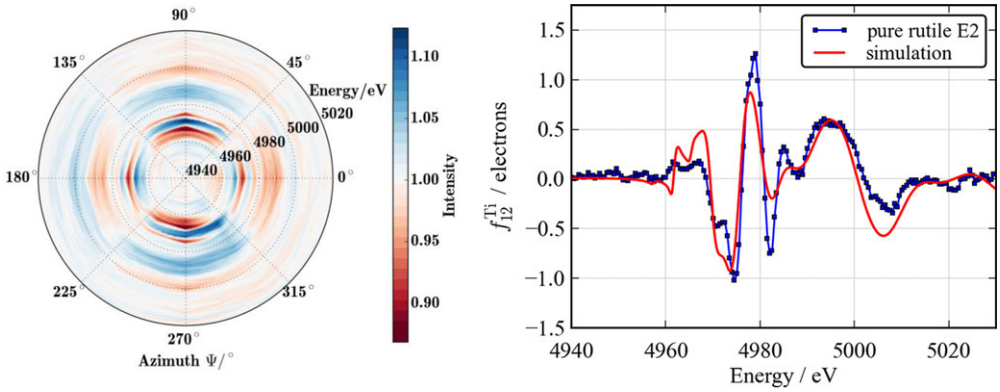

Fig. 7 Energy and azimuthal dependence of the "partially forbidden" rutile 111 reflection intensity from a DAFS-AAS measurement (left) showing the mirror symmetry at $\psi = 0°$ and 180°. Destructive interference cancels the isotropic Ti scattering contribution, whereas an isotropic contribution from the oxygen partial structure interferes with the anisotropic scattering part of Ti, yielding its absolute value and sign. The experimentally determined spectrum of the titanium scattering tensor component f'_{12} (right) shows a good agreement with *ab initio* calculations performed with FDMNES [77] (red line).

octahedrally coordinated by oxygen atoms with a slight elongation of the binding distance in the basal planes and a higher O-Ti-O angle in [110] than in [001], which cancels the degeneracy for all p-orbitals.

We investigated "forbidden" as well as "partially forbidden" reflections where the isotropic structure amplitude is zero for all scatterers within the structure or only for a part of the crystallographic sites (here the Ti site). The reflections have been chosen to have a maximum polarization dependency, due to anisotropy in the titanium scattering amplitude near the Ti *K*-edge, represented solely by the dipole-dipole tensor component $f^{d}{}_{12}$. The DAFS measurements have been carried out at beamlines P09 of Petra-III and E2, W1 of Doris-III (DESY-PhotonScience, Hamburg) [96–98], and were separated from the smooth energy dependency extracting the relative oscillations only.

To investigate exclusively the anisotropy of the unoccupied electronic Ti states and eliminate all isotropic scattering contributions, the "forbidden" 001 reflection has been chosen, based on a theoretic model of Dmitrienko [34] and proven experimentally by Kirfel and Petcov [37]. The ψ-dependency perfectly reflects a 4-fold rotational symmetry along the 4_2-axis originating from p-orbitals of the O-Ti-O bonding units in *c*-plane at $c = 0$ and $c = {}^1/_2$ (see figure 6). Intensity maxima occur in the $\sigma - \sigma'$ channel for $\psi = 45°$, 135°, 225° and 315°, whenever the incident polarization vector points towards an oxygen atom neighboring the resonant titanium atom. In the case of the flipped $\sigma - \pi'$ polarization channel, maxima and minima are interchanged (transverse field polarization states σ orthogonal to and π within the scattering plane).

Furthermore, AAS can be used to directly determine the phase of the resonant scatterer by means of "partially forbidden" reflections. In our case, the 111 reflection has been chosen where, again, the isotropic contributions of the Ti partial structure cancel out by destructive interference, but the oxygen partial structure adds a constant scattering contribution to the structure factor. This contribution acts as a known reference wave and interferes with the purely resonant scattering contribution from the titanium atoms. Using this, the absolute value and phase of the tensor component $f^{d}{}_{12}$ of the titanium scattering amplitude can be extracted by fitting the azimuthal dependencies (see figure 7) according to

$$I_{\sigma\sigma'} \propto c^2 \cdot |f^{O}|^2 + \xi(\psi)^2 \left| f_{12}^{Ti} \right|^2 + 2c \cdot \xi(\psi) \left(\mathrm{Re}(f^{O}) \mathrm{Re}(f_{12}^{Ti}) + \mathrm{Im}(f^{O}) \mathrm{Im}(f_{12}^{Ti}) \right) \quad (2)$$

where $\xi(\psi)$ describes the azimuthal dependence, c is energy dependent and f^{O} is the isotropic scattering amplitude of oxygen. It can be seen in equation (2) that the resulting imaginary part of the tensor component is subject to a large error, because it is weighted with the relatively small imaginary part of the oxygen scattering amplitude, whereas the real part of the tensor component dominates the measured spectra, since it is weighted by the considerably large real part of oxygen. It has to be mentioned that a strong relative azimuthal signal can only be expected if the isotropic part originates from a weak scatterer as in this case is oxygen. Otherwise the anisotropy is suppressed.

CRYSTAL Research & Technology

6 Summary

Resonant X-ray Scattering and *Diffraction Anomalous Fine Structure* can be used to obtain local structural and electronic information about a specific atomic species in a crystal. Moreover, it combines spectroscopy with the wavevector and site selectivities of long-range order based diffraction and thus allows distinguishing between the local structure of the same element in different structural phases or symmetry positions within a crystal. By means of polarization analysis, even the sensitivity to probe specific orbitals is given, which addresses the local site symmetry of the Wyckoff position. The angular momentum of X-ray photons can be used to change the electron's spin moment and to study magnetism. In theory, resonant diffraction and absorption are closely related and dependent upon another, and a self-consistent analysis of both is therefore highly beneficial in respect to experimental data reduction and absorption correction as well as *ab initio* simulation and interpretation. With nowadays dedicated photon science storage rings, resonant scattering experiments are in general feasible for any crystalline structure. Still, the analysis and the interpretation remain complex and the methods have not reached the status of standard high-throughput techniques yet.

This condensed review presents pioneer work in the field of *Resonant X-ray Diffraction* methods with an overview on theory and experiment and a selection of exemplary applications in order to give an understanding of their powerful sensitivities. To provide an exhaustive summary on the vast amount of studies using *Resonant X-ray Diffraction* would require several volumes and is beyond the scope of this review. A selection of recent related publications is chosen with special focus on *Diffraction Anomalous Fine Structure* and *Anisotropy of Anomalous Scattering*. Some recent results of the authors on rutile TiO_2 are included to demonstrate the progress in measurement technique and data analysis.

Acknowledgments. The authors would like to thank Dr. D. V. Novikov, Prof. K. Fischer, Prof. V. E. Dmitrienko and Dr. E. N. Ovchinnikova for their support and fruitful discussions. We thank the DFG for financial support within the cooperative project ME 1433/10–1, GE 1202/8–1, the BMBF within project 05K10OF1 and the SAB within the Landesinnovationsstipendium 100 111 044.

Key words. diffraction anomalous fine structure, anisotropic anomalous scattering, resonant elastic X-ray scattering, forbidden reflection near-edge diffraction.

References

[1] V. Scagnoli, U. Staub, A. M. Mulders, M. Janousch, G. I. Meijer, G. Hammerl, J. M. Tonnerre, and N. Stojic, Phys. Rev. B **73**, 100409(R) (2006).
[2] W. A. Hendrickson and C. M. Ogata, Method. Enzymol. **276**, 494 (1997).
[3] J. M. Bijvoet, Proc. K. Ned. Akad. Wet. Ser. B **52**, 313 (1949).
[4] U. W. Arndt, T. J. Greenhough, J. R. Helliwell, J. A. K. Howard, S. A. Rule, and A. W. Thompson, Nature **298**, 835 (1982).
[5] J. P. Attfield, Mater. Sci. Forum **228**, 201 (1996).
[6] U. Vainio, K. Pirkkalainen, K. Kisko, G. Georigk, N. E. Kotelnikova, and R. Serimaa, Eur. Phys. J. D **42**(1), 93 (2007).
[7] H. Fricke, Phys. Rev. **16**, 202 (1920).
[8] D. E. Sayers, E. A. Stern, and F. W. Lytle, Phys. Rev. Lett. **27**, 1204 (1971).
[9] P. Eisenberger and B. Kincaid, Science **200**, 1441 (1978).
[10] J. J. Rehr and A. L. Ankudinov, Coordin. Chem. Rev. **249**, 131 (2005).
[11] V. L. Aksenov, M. V. Koval'chuk, A. Y. Kuz'min, Y. Purans, and S. I. Tyutyunnikov, Crystallogr. Rep. **51**, 908 (2006).
[12] W. A. Hendrickson, Trans. Am. Crystallogr. Assoc. **21**, 11 (1985).
[13] Y. Cauchois, C. R. Acad. Sci. (Paris) **242**, 100 (1956).
[14] D. H. Templeton and L. K. Templeton, Acta Cryst. A **36**, 237 (1980).
[15] V. Ponomarev and Y. A. Turutin, Sov. Phys.-Tech. Phys. **28**, 232 (1984).
[16] I. Arčon, A. Kodre, D. Glavič and M. Hribar, J. Phys. Colloques **48**, C9–1105 (1987).
[17] H. Stragier, J. O. Cross, J. J. Rehr, L. B. Sorensen, C. E. Bouldin, and J. C. Woicik, Phys. Rev. Lett. **69**, 3064 (1992).
[18] I. J. Pickering, M. Sansone, J. Marsch, and G. N. George, J. Am. Chem. Soc. **115**, 6302 (1993).
[19] L. B. Sorensen, J. O. Cross, M. Newville, B. Ravel, J. J. Rehr, H. Stragier, C. E. Bouldin, and J. C. Woicik, in: Resonant Anomalous X-ray Scattering: Theory and Applications, Eds. G. Materlik, C. J. Sparks and K. Fischer, North-Holland, Amsterdam 1994, p. 389.
[20] W. Morgenroth, A. Kirfel, and K. Fischer, Z. Kristallogr. **209**, 124 (1994).
[21] J. O. Cross, Analysis of Diffraction Anomalous Fine Structure, Diss., University of Washington 1996.
[22] H. Renevier, J. L. Hodeau, P. Wolfers, S. Andrieu, J. Weigelt, and R. Frahm, Phys. Rev. Lett. **78**, 2775 (1997).
[23] D. C. Meyer, K. Richter, A. Seidel, J. Weigelt, R. Frahm, and P. Paufler, J. Synchrotron Rad. **5**, 1275 (1998).
[24] A. Kirfel and K. Fischer, Z. Kristallogr. **213**, 337 (1998).
[25] J. C. Woicik, J. O. Cross, C. E. Bouldin, B. Ravel, J. G. Pellegrino, B. Steiner, S. G. Bompadre, L. B. Sorensen, K. E. Miyano, and J. P. Kirkland, Phys. Rev. B **58**, R4215 (1998).

CRYSTAL Research & Technology

[26] D. C. Meyer, K. Richter, P. Paufler, and G. Wagner, Phys. Rev. B **59**, 15253 (1999).
[27] J.-L. Hodeau, V. Favre-Nicolin, S. Bos, H. Renevier, E. Lorenzo, and J.-F. Berar, Chem. Rev. **101**, 1843 (2001).
[28] J. P. Hannon, G. T. Trammell, M. Blume, and D. Gibbs, Phys. Rev. Lett. **61**, 1245 (1988).
[29] H. Renevier, S. Grenier, S. Arnaud, J. F. Bérar, B. Caillot, J. L. Hodeau, A. Letoublon, M. G. Proietti, and B. Ravel, J. Synchrotron Rad. **10**, 435 (2003).
[30] D. H. Templeton and L. K. Templeton, Acta Cryst. A **36**, 237 (1980).
[31] D. H. Templeton and L. K. Templeton, Acta Cryst. A **38**, 62 (1982).
[32] International Tables for Crystallography. Vol. A: Space-group symmetry, 5th Edition, Eds. T. Hahn, Kluwer Academic Publishers, Dordrecht 2002.
[33] Resonant Anomalous X-ray Scattering: Theory and Applications, Eds. G. Materlik, C. J. Sparks, and K. Fischer, North-Holland, Amsterdam 1994.
[34] V. E. Dmitrienko, Acta Cryst. A **39**, 29 (1983).
[35] D. H. Templeton and L. K. Templeton, Acta Cryst. A **41**, 133 (1985).
[36] K. Eichhorn, A. Kirfel, and K. F. Fischer, Z. Naturforsch. A, **43**(4) 391 (1988).
[37] A. Kirfel and A. Petcov, HASYLAB/DESY Annual Report, 385 (1989).
[38] V. E. Dmitrienko, K. Ishida, A. Kirfel, and E. N. Ovchinnikova, Acta Cryst. A **61**, 481 (2005).
[39] T. A. W. Beale, G. Beutier, S. R. Bland, A. Bombardi, L. Bouchenoire, O. Bunău, S. Di Matteo, J. Fernández-Rodríguez, J. E. Hamann-Borrero, J. Horrero-Martín, V. L. R. Jacques, R. D. Johnson, A. Juhin, T. Matsumura, C. Mazzoli, A. M. Mulders, H. Nakao, J. Okamoto, S. Partzsch, A. J. Princep, V. Scagnoli, J. Strempfer, C. Vecchini, Y. Wakabayashi, H. C. Walker, D. Wermeille, and Y. Yamasaki, Eur. Phys. J. Special Topics **208**, 89 (2012).
[40] U. Staub, Y. Bodenthin, C. Piamonteze, S. P. Collins, S. Koohpayeh, D. Fort, and S. W. Lovesey, Phys. Rev. B **82**, 104411 (2010).
[41] M. García-Fernández, U. Staub, Y. Bodenthin, V. Pomjakushin, A. Mirone, J. Fernández-Rodríguez, V. Scagnoli, A. M. Mulders, S. M. Lawrence, and E. Pomjakushina, Phys. Rev. B **82**, 235108 (2010).
[42] C. Azimonte, E. Granado, H. Terashita, S. Park, and S.-W. Cheong, Phys. Rev. B **81**, 012103 (2010).
[43] T. A. W. Beale, S. B. Wilkins, R. D. Johnson, S. R. Bland, Y. Joly, T. R. Forrest, D. F. McMorrow, F. Yakhou, D. Prabhakaran, A. T. Boothroyd, and P. D. Hatton, Phys. Rev. Lett. **105**, 087203 (2010).
[44] R. A. de Souza, U. Staub, V. Scagnoli, M. Garganourakis, Y. Bodenthin, S.-W. Huang, M. García-Fernández, S. Ji, S.-H. Lee, S. Park, and S.-W. Cheong, Phys. Rev. B **84**, 104416 (2011).
[45] H. C. Walker, F. Fabrizi, L. Paolasini, F. de Bergevin, J. Herrero-Martin, A. T. Boothroyd, D. Prabhakaran, and D. F. McMorrow, Science **333**, 1273 (2011).
[46] V. E. Dmitrienko and V. A. Chizhikov, Phys. Rev. Lett. **108**, 187203 (2012).
[47] M. Guarise, B. D. Piazza, M. M. Sala, G. Ghiringhellim, L. Braicovich, H. Berger, J. N. Hancock, D. Van der Marel, T. Schmitt, V. N. Strocov, L. J. P. Ament, J. Van den Brink, P.-H. Lin, P. Xu, H. M. Rønnow, and M. Grioni, Phys. Rev. Lett. **105**, 157006 (2010).
[48] M. W. Haverkort, N. Hollemann, I. P. Krug, and A. Tanaka, Phys. Rev. B **82**, 094403 (2010).
[49] G. L. Pascut, R. Coldea, P. G. Radaelli, A. Bombardi, G. Beutier, I. I. Mazin, M. D. Johannes, and M. Jansen, Phys. Rev. Lett. **106**, 157206 (2011).
[50] J. Herrero-Martín, J. Blasco, J. García, G. Subías, and C. Mazzoli, Phys. Rev. B **83**, 184101 (2011).
[51] M.-H. Tuilier, M.-J. Pac, D. V. Anokhin, D. A. Ivanov, C. Rousselot, and D. Thiadaudière, Thin Solid Films **526**, 2690 (2012).
[52] V. Favre-Nicolin, M. G. Proietti, C. Leclere, N. A. Katcho, M.-I. Richard, and H. Renevier, Eur. Phys. J. Special Topics **208**, 189 (2012).
[53] E. Piskorska-Hommel, V. Holý, O. Caha, A. Wolska, A. Gust, C. Kruse, H. Kröncke, J. Falta, and D. Hommel, J. Alloy Compd **523**, 155 (2012).
[54] H. C. Walker, R. Caciuffo, D. Aoki, F. Bourdarot, G. H. Lander, and J. Flouquet, Phys. Rev. B **83**, 193102 (2011).
[55] H. C. Walker, M. D. Le, K. A. McEwen, M. Bleckmann, S. Süllow, C. Mazzoli, S. B. Wilkins, and D. Fort, Phys. Rev. B **84**, 235142 (2011).
[56] M. A. Hossain, B. Bohnenbuck, Y. D. Chuang, M. W. Haverkort, I. S. Elfimov, A. Tanaka, A. G. Cruz Gonzalez, Z. Hu, H.-J. Lin, C. T. Chen, R. Mathieu, Y. Tokura, Y. Yoshida, L. H. Tjeng, Z. Hussain, B. Keimer, G. A. Sawatzky, and A. Damascelli, Phys. Rev. B **86**, 041102(R) (2012).
[57] M. A. Hossain, I. Zegkinoglou, Y.-D. Chuang, J. Geck, B. Bohnenbuck, A. G. Cruz Gonzalez, H.-H. Wu, C. Schüßler-Langeheine, D. G. Hawthorn, J. D. Denlinger, R. Mathieu, Y. Tokura, S. Satow, H. Takagi, Y. Yoshida, Z. Hussain, B. Keimer, G. A. Sawatzky, and A. Damascelli, Sci. Rep. **3**, 1 (2012).
[58] J. Kokobun and V. E. Dimitrienko, Eur. Phys. J. Special Topics **208**, 39 (2012).
[59] C. Vettier, Eur. Phys. J. Special Topics **208**, 3 (2012).
[60] G. H. Lander, Eur. Phys. J. Special Topics **208**, 129 (2012).
[61] Y. Joly, S. D. Matteo, and O. Bunău, Eur. Phys. J. Special Topics **208**, 21 (2012).
[62] C. Detlefs, M. Sanchez del Rio, and C. Mazzoli, Eur. Phys. J. Special Topics **208**, 359 (2012).
[63] R. W. James, The Optical Principles of the Diffraction of X-rays, Ox Bow Press, Woolbridge 1982.
[64] L. G. Parratt and C. F. Hempstead, Phys. Rev. **94**, 1593 (1954).
[65] D. T. Cromer, Acta Cryst. **18**, 17 (1965).
[66] D. T. Cromer and D. Liberman, J. Chem. Phys. **53**, 1891 (1970).
[67] A. G. McKale, B. W. Veal, A. P. Paulikas, S.-K. Chan, and G. S. Knapp, J. Am. Chem. Soc. **110**, 3763 (1988).
[68] A. V. Kolpakov, V. A. Bushuev, and R. N. Kuzmin, Sov. Phys. Uspekhi **126**, 479 (1978).

CRYSTAL Research & Technology

[69] C. R. Natoli, M. Benfatto, C. Brouder, M. F. Ruiz López, and D. L. Foulis, Phys. Rev. B **42**, 1944 (1990).
[70] J. J. Rehr, R. C. Albers, and S. I. Zabinsky, Phys. Rev. Lett. **69**, 3397 (1992).
[71] J. O. Cross, M. Newville, J. J. Rehr, L. B. Sorensen, C. E. Bouldin, T. Gouder, G. H. Lander, and M. I. Bell, Phys. Rev. B **58**, 11215 (1998).
[72] G. Wendin, Phys. Scripta **21**, 535 (1980).
[73] J. J. Rehr and R. C. Albers, Rev. Mod Phys. **72**, 621 (2000).
[74] A. L. Ankudinov and J. J. Rehr, Phys. Rev. B **62**, 2437 (2000).
[75] M. Benfatto and R. Felici, Phys. Rev. B **64**, 115410 (2001).
[76] Y. Joly, Phys. Rev. B **63**, 125120 (2001).
[77] Y. Joly, S. P. Collins, S. Grenier, H. C. N. Tolentino, and M. De Santis, Phys. Rev. B **86**, 220101(R) (2012).
[78] O. Bunău and Y. Joly, J. Phys.: Condens. Matter **21**, 345501 (2009).
[79] U. Ekström, P. Norman, V. Carravetta, and H. Ågren, Phys. Rev. Lett. **97**, 143001 (2006).
[80] J. J. Rehr, Radiat. Phys. Chem. **75**, 1547 (2005).
[81] K. Hümmer, E. Weckert, and H. Bondza, Acta Cryst. A **45**, 182 (1989).
[82] S. Francoual, J. Strempfer, D. Reuther, D. K. Shukla, and A. Skaugen, J. Phys. Conf. Ser. **425**, 132010 (2013).
[83] U. Bonse and K. Fischer, Nuclear Instruments and Methods in Physics Research **190**, 593 (1981).
[84] B. Dawson, in: Advances in Structure Research by Diffraction Methods, Eds. W. Hoppe and R. Mason, Volume **6**, Vieweg, Braunschweig 1975.
[85] V. E. Dmitrienko and E. N. Ovchinnikova, Acta Cryst. A **56**, 340 (2000).
[86] V. E. Dmitrienko and E. N. Ovchinnikova, J. Synchrotron Rad. **10**, 376 (2003).
[87] K. Hirota, N. Oumi, T. Matsumura, H. Nakao, Y. Wakabayashi, Y. Murakami, and Y. Endoh, Phys. Rev. Lett. **84**, 2706 (2000).
[88] E. N. Ovchinnikova, V. E. Dmitrienko, K. Ishida, A. Kirfel, S. P. Collins, A. P. Oreshko, D. Cabaret, R. V. Vedrisnkii, V. L. Kraizman, A. A. Novakovich, E. V. Krivitskii, and B. P. Tolochko, Nucl. Instrum. Methods A **543**, 122 (2005).
[89] V. E. Dmitrienko and E. N. Ovchinnikova, Struct. Chem. **13**, 397 (2002).
[90] Y. Murakami, J. P. Hill, D. Gibbs, M. Blume, I. Koyama, M. Tanaka, H. Kawata, T. Arima, Y. Tokura, K. Hirota, and Y. Endoh, Phys. Rev. Lett. **81**, 582 (1998).
[91] E. N. Ovchinnikova and V. E. Dmitrienko, Acta Cryst. A **56**, 2 (2000).
[92] Y. Tanaka, T. Takeuchi, S. W. Lovesey, K. S. Knight, A. Chainani, Y. Takata, M. Oura, Y. Senba, H. Ohashi, and S. Shin, Phys. Rev. Lett. **100**, 145502 (2008).
[93] E. Nazarenko, J. E. Lorenzo, Y. Joly, J. L. Hodeau, D. Mannix, and C. Marin, Phys. Rev. Lett. **97**, 056403 (2006).
[94] J. E. Lorenzo, C. Mazzoli, N. Jaouen, C. Detlefs, D. Mannix, S. Grenier, Y. Joly, and C. Marin, Phys. Rev. Lett. **101**, 226401 (2008).
[95] Y. Tanaka and S. W. Lovesey, Eur. Phys. J. Special Topics **208**, 67 (2012).
[96] M. Zschornak, T. Leisegang, E. Gutmann, H. Stöcker, D. V. Novikov, K. Rickers, and D. C. Meyer, HASYLAB/DESY Annual Report, 973 (2007).
[97] M. Zschornak, H. Stöcker, T. Leisegang, C. Richter, S. Gemming, D. V. Novikov, and D. C. Meyer, HASYLAB/DESY Annual Report, 162 (2008).
[98] C. Richter, M. Zschornak, J. Schulze, D. V. Novikov, and D.C. Meyer, HASYLAB/DESY Annual Report, 324 (2010).